BIDIRECTIONAL OPTICAL PROPERTIES OF SLAT SHADING: COMPARISON BETWEEN RAYTRACING AND RADIOSITY METHODS

M. RUBIN*, J. JONSSON, C. KOHLER, J. KLEMS

Windows and Daylighting Group, Building Technologies Program, Lawrence Berkeley National Laboratory, 1 Cyclotron Road, Berkeley, CA 94720, U.S.A.

D. CURCIJA AND N. STOJANOVIC

Carli Inc., Amherst, MA, U.S.A.

July 11, 2007

ABSTRACT

The Window 6.0 computer program incorporates a model for calculating the optical properties and solar heat gain factor of slat shading systems. This model adheres to the framework appearing in the ISO 15099 standard, which is based on a radiosity approach. Only the directional-hemispherical properties of the slat shading can be predicted by the method of ISO 15099. Extensions to the Window 6.0 implementation enable the calculation in full bidirectional detail. A detailed raytracing model based on a Monte-Carlo method is compared to the Window 6.0 radiosity implementation. Directional-hemispherical values are in excellent agreement for all conditions. Bidirectional results are in good qualitative agreement. Simplifying assumptions in the Window 6.0 model such as zero-thickness slats and segmented slat curvature are shown

* Corresponding Author, email: MDRubin@LBL.gov, fax: 510.486.7124

to have little detrimental effect except in certain cases. One significant limitation of the radiosity approach is the inability to model specular slat properties.

KEYWORDS

Windows, shading, raytracing, radiosity

INTRODUCTION

The Window 5.2 computer program developed by LBNL is widely used to calculate the thermal and optical properties of windows. Research version 6.0 (Mitchell et al., 2006) includes the possibility to model diffusing and light-redirecting glazing and shading elements. Given the full bidirectional transmittance and reflectance of each "planar" layer (e.g., glass or slat shading system), Window 6.0 can calculate the bidirectional transmittance and reflectance of the assembly of layers using the matrix method of Klems (1994). One (extremely tedious) way to obtain the data for slat-shading systems would be to measure many such products, not only as a function of incident and emerging angles, but also for varying colors, slat width, spacing, curvature and tilt angle. A more efficient route is provided in Window 6.0 by inclusion of a specific model of slat-shading systems which requires only the geometry of the slats and their reflectance as input.

The Window 6.0 slat-shading model adheres to the ISO 15099 standard (ISO, 2002), Section 7.3, which uses the form-factor or radiosity approach. The radiosity method is one of the most common techniques used by heat-transfer engineers to predict the flow of radiation among surfaces in a complex geometrical system; see, for example, Siegel and Howell (1978). ISO 15099 was written with the intention of providing a

framework rather than a prescriptive standard. Different implementations may therefore give different results depending on choice of environmental conditions and other model parameters. Furthermore, the ISO slat model makes a number of simplifying assumptions: Slats must be flat and have zero thickness. Also, slat surfaces are assumed to have Lambertian (uniformly diffuse) reflectance as in all radiosity models.

As available computational power grows, Monte-Carlo raytracing is an increasingly popular option for determining the properties of complex fenestration systems. Raytracing as a general technique in radiation heat transfer is also described in many textbooks such as Siegel and Howell. Raytracing overcomes some of the inherent limitations of the radiosity method. In particular, surfaces may have both specular and diffuse properties in raytracing, which we will find useful later. Lack of detailed optical properties for slat surfaces is one of the main deficiencies in calculations of slat-shading properties in studies to date.

Validation of a computational model is perhaps best fulfilled by a careful experimental study. In the case of optical properties of complex fenestration systems, however, experimental validation is compromised by the scarcity of instruments for measuring large-scale systems and the lack of standards for their operation. Furthermore, the single organized interlaboratory comparison to date (Platzer, 2000) did not result in close agreement between available instruments for the most complex systems. Under the circumstances, if any two methods agree, even two different computational methods, this must be considered a promising event. We will also cite some indirect experimental validation of our raytracing model, which is further cause for optimism.

In this paper we first describe our two computational approaches based on radiosity and raytracing. Then we compare results from the two approaches for several blind systems listed in ISO 15099. Finally we explore some of the simplifying assumptions of the ISO-derived model. In particular we measure the reflectance of some real slat materials which generally have some specular component as well as some dependence on wavelength and polarization.

THE WINDOW 6.0 RADIOSITY MODEL

Parmelee and Aubele (1952) applied a radiosity method to describe slat systems which they verified by solar calorimetry. The results of this remarkable work, accomplished in the days before electronic computers, were reduced to a simple tabular form.. Thirty-three years later Mitts and Smith (1985) would extend the model, complete with full text of their Fortran code. Incident radiation is treated as either directly transmitted, converted from beam to diffuse upon reflection from a slat, or preserved as diffuse upon reflection from a slat. Van Dijk and Bakker (1998) emphasized this "beam-diffuse" aspect in work that led to the ISO 15099 standard.

Carli (2006) implemented a version of the ISO 15099 slat model for Window 6.0. The reader interested in doing their own calculations will find all necessary description of coordinate systems, slat geometry, form factors, and property matrices provided in the report. Although the specifics of that report go far beyond the level of detail in ISO 15099, the general method is well known and we shall not describe it further here. An extension of the base model (Klems, 2004b, 2005) permits Window 6.0 to parse the directional-hemispherical transmission and reflection into the respective bidirectional

properties, which are sometimes required for detailed distribution of heat or daylight in a room. In any case, Window 6.0 requires the bidirectional data of each layer to perform its matrix calculation for the overall properties of the multilayer system. Because the Klems bidirectional extension is specialized and as yet unpublished we explain it here:

The simplest method for distributing the transmitted flux simply treats the slat-shading "layer" as if it was a Lambertian surface with constant radiance in all directions. Obviously this will not be correct for a Venetian blind with its highly nonuniform distribution of light. The next level of refinement takes into account which segments are "visible" and which segments are "shielded" by other slats when considered at the outgoing angle, i.e., the radiation intensity at a given angle is adjusted by consideration of the cut-off angle.

Figure 1 shows how the outgoing radiance (and hence transmittance) changes with outgoing profile angle, for a simple case of a flat-slat Venetian blind. The blind is irradiated by light that arrives at an incident profile angle ψ_{in}. The incident radiation is diffusely reflected off both slats. When the radiation reaches the indoor facing imaginary plane, four different bands can be identified for outgoing directions which lay in a vertical plane, starting from the lowest outgoing angle of -90° (-π/2):

1. Increasing radiance – the total outgoing radiance increases with ψ_{out}, from zero to $I_{\max,1}$, achieved at outgoing angle $\psi_{\max 1}$, as a larger part of the upper slat becomes visible.
2. Decreasing radiance, as angle between outgoing direction and upper slat normal vector decreases, from $\psi_{\max 1}$ to zero at slat tilt angle ψ_{slat}

3. Increasing radiance – when ψ_{out} increases past slat tilt angle ψ_{slat}, lower slat is no longer visible, and lower slat becomes completely visible, outgoing radiance increases from zero to $I_{max,2}$, which is achieved at outgoing angle $\psi_{max\,2}$
4. Decreasing radiance – as outgoing angle increases past $\psi_{max\,2}$, decrease of total visible part of the lower slat outweights the decrease of angle between outgoing direction and normal vector of the lower slat in terms of an overall contribuiton to outgoing radiance, which results in decreasing of the total outgoing radiance from $I_{max,2}$, to zero for $\psi_{out} = -90°$ $(-\pi/2)$.

Figure 2 plots the outgoing radiance against outgoing profile angle, for the example above. Notice that I_1 has a higher value than I_2, because I_1 contains a part of radiation that is reflected only once (off the lower slat), which is not the case with I_2. The energy-balance equations among slat segments and the environment (represented by imaginary vertical bounding planes) are similar to those of ISO 15099 with the following exceptions: Unlike the basic enclosure model there are no virtual segments for the front and back opening; therefore, the dimension of this system is reduced by 2. The system of equations is formed and solved for radiosities leaving slat segments, instead of irradiances arriving at slat segments. The resulting outgoing radiation is calculated as a sum of contributions of each segment of the two adjacent slats, using radiosities leaving each slat segment instead of irradiance reaching the imaginary vertical boundaries.

THE MONTE-CARLO RAYTRACING METHOD

An early application of Monte-Carlo techniques to Venetian blinds was performed by Campbell and Whittle (1997) who developed their own raytracer. Kuhn et al. (2001), adapted one of the general commercial raytracing programs. We have chosen to use TracePro® by Lambda Research Corp. (www.lambdares.com). TracePro® is sufficiently easy to use, although all such programs are necessarily complex because they are intended for the design of optical systems with the widest possible range of configurations and properties. Using the CAD interface, we can easily make a geometrical description of a slat shading system. TracePro® has a Scheme-based scripting language with raytracing extensions that makes it possible to automate the entire process.

TracePro® has been used and validated for a wide variety of optical applications. Assuming that we use the program properly, and provide accurate input data, there is every reason to believe that our results will be accurate. Experimental results from a large-scale goniophotometer were compared to earlier raytracing results of a slat shading system (Anderson, et al., 2005a) as well as a prismatic panel system with some similar characteristics to blinds (Anderson, et al., 2005b). Since then our raytracing process has been reconfigured and automated, but the general operating principles are still the same. Thus we consider the earlier results to be meaningful, if indirect, experimental validation of our current raytracing studies.

A Scheme macro has been written not only to perform a sequence of tests and process the results, but also to construct detector spheres, place sources at appropriate input angles, and generate the slat systems in a visual analog to a real instrument. This

"virtual" goniospectromter (VGS) can be preserved and brought forth for later use or transferred to new users with guaranteed repeatable results. The current version of our macro VGS 2.0, used for this study, is highly configurable with respect to light source and sample geometry. Therefore care must be taken so that the raytracing set-up properly simulates the case which is studied. For example, comparing raytracing with the ISO 15099 results requires a rectangular light spot with a height equal to the slat spacing and also a slat thickness of zero. Unlike a real instrument the VGS is freed from inconvenient material limitations and we can construct a VGS with capabilities unlike anything that could be practically built in the laboratory as described below.

For capturing detailed bidirectional optical data in spherical coordinates, which is the natural coordinate system for this application, the ideal detector would be a spherical shell divided into a number of flux-collecting segments. A virtual detector sphere has many advantages over physical counterparts. The cost for a detector surface covering the inside of a 2-meter sphere would be prohibitive. For this reason real detectors are small and often mounted on the end of a moving arm, although there are some clever implementations using projection screens and cameras. Also, the detector surfaces can be made perfectly transparent thereby eliminating stray reflected light. There are no supports for the detector (or sample holder) to block light at low angles of incidence. Furthermore, we may wish to vary the diameter of the sphere for near and far field measurements, which could not be done experimentally.

Using the VGS 2.0 script, a detector sphere can be divided into segments along the altitude θ and azimuth φ coordinates with the desired resolution. This operation is performed by Boolean subtraction of planes from a spherical shell. A typical result of

this operation appears in Figure 3. The angular basis set of Tregenza (1987) was adopted by the International Energy Agency Task 21 and Task 31 on daylighting. In this work, we use the modified basis set devised by Klems (2004a), which has some advantages in terms of maximizing resolution where it is needed. Window 6.0 can accept data with any angular basis set but we hope that an international standard will emerge.

Next the macro constructs the light sources. In a physical instrument the source and/or sample would have to move or be directed through the entire hemisphere. In the virtual world we can make the center of each detector patch into a light-emitting surface. This is convenient because the detector patches are already defined, but it would become tedious without a script since there are more than a hundred incident directions. It is required that the same area of the sample is illuminated with constant irradiance for each incident angle. There will be a small movement where the rays hit the sample since the origin of the rays is changed, but this can be neglected since the virtual detector sphere can be made arbitrarily much larger than the sample. A linear random process is used to determine exactly where in the light spot each individual ray travels ensuring a constant irradiance over the area. Another possibility, used in our earlier work, is to make a single source plane parallel and adjacent to the sample and launch the rays in the desired direction.

Compared to the time it takes to trace millions of rays, the VGS can be regenerated by a script very quickly. So we actually recreate the instrument for each run because this is much easier than going into the solid-model interface and manually making changes or saving many configurations. The macro amounts to a specialized interface to TracePro® for specification of the system parameters. For example, we can

create a Venetian blind (Figure 4) simply by specifying a few numbers such as slat width and spacing; the user doesn't even need to learn to use the CAD tools, menu commands or interact directly with TracePro®.

EXPERIMENTAL DETERMINATION OF SLAT REFLECTANCE

Little data is available on the experimental reflectance of slat materials; most studies to date treat this important characteristic as a variable parameter. In fact, we shall do the same thing because in comparing our results to others we must use the reflectance values assumed in those other studies. Nevertheless we shall also begin to look at real slat reflectance if only to assure ourselves that we are using reasonable values and to establish the need for further experimental work. For this purpose, we measured the reflectance of nine slat materials; most were painted aluminum strips, one was a more specular brushed metallic surface with a gold color, and one was a highly specular Al-coated slat. Flat samples were obtained from the manufacturer before cutting and rolling to avoid focusing effects in measurement.

The sample is placed flush against the reflectance port of the sphere with the light beam incident at 8 degrees. Another port can be opened at the position where a specularly reflected beam would strike the sphere wall to trap the specular component of the reflected light. In this way we can obtain the total and diffuse reflectance, or, by subtraction the specular reflectance. We will carefully define the term "specular" for this case because the trapped beam will not only include true specular reflection but also a small amount of diffusely reflected light encompassed by the trap. Our light trap is a rectangle 33 mm by 35 mm subtending a half angle of 6.4° and 6.7°, respectively, around the specular direction.

The painted slat slats of various colors have a wide range of reflectance in the visible (see Figure 5) as would be expected. Some have a fairly high degree of selectivity which indicates that it might be important to include wavelength dependence rather than integrated values in order to properly calculate window system properties. Reflectance generally trends higher into the solar infrared but varies widely rather than approaching a common value for the binder material.. The white surface is highly reflective over the entire solar spectrum; it is even more reflective than the brushed golden metal surface in the visible. Assuming for now that the reflectance is purely diffuse, we find that the examples from ISO 15099 are fairly realistic, ie., the solar reflectance of the white slat is about 0.7 and for the green slat about 0.4. There are other types of surface treatment sometimes used that are even more reflective. Brushed Al with and without an enhancing coating have a total reflectance of 0.9 and 0.95 respectively.

Figure 6 shows the result of subtracting the diffuse component from the total, giving what we shall call the specular component. Painted slats, despite a sometimes noticeable glossy appearance, have specular reflection less than 5% in the visible with a gradual increase in the solar infrared. The red pigment presents a small but interesting deviation from the general trend; specular reflection in the visible is on the low side but increases to approximately double that of any other pigment in the infrared. Parmelee et al. (1953) found a similar result for their white slat material (total reflectance 0.75 and diffuse reflectance 0.3) using an integrating sphere with light trap of unspecified configuration. The brushed gold-colored surface has a significantly higher specular component, but still a relatively small fraction of the total. Al-coated slats have a much higher specular component, close to the total reflectance. So, the assumption that slat

reflectance is completely diffuse is approximately correct for conventional painted surfaces but in at least one special case the specular component can also range to high levels. Such specularly reflecting slats are usually intended as light-redirecting devices for improving the utilization of daylight in commercial buildings rather than simply as shading devices.

At this point studies often implicitly assume that the slat reflectance is Lambertian in the broadest sense, i.e., that the reflectance is independent of either incoming or outgoing angles. Parmelee et al. (1953) showed that this is approximately true for the outgoing diffuse component at one angle of incidence at least. We will further examine the dependence on incident angle. Measuring direct-hemispherical reflectance versus angle of incidence correctly is not trivial and we must now work without benefit of standard instruments and procedures. Two different experimental set-ups were used for comparison as described below.

The first technique uses a custom-built reflectance sphere situated in the Ångström Laboratory at Uppsala Univ., which was designed specifically for this kind of measurement. It is thoroughly described by Nostell et al. (1999); a brief description follows: There is only one port, the entrance port. The sample is situated on a rotating sample holder in the middle of the sphere, the rotating axis goes out through the top of the sphere where it is connected to a stepper motor. The detector is positioned in the sample holder with a field of view covering the bottom of the sphere, so that no directly reflected light is ever seen by the detector, regardless of angle of incidence. The sphere wall is covered with barium sulfate paint. The light source is a halogen tungsten lamp

which in combination with two gratings produces monochromatic light from 300 nm to 2550 nm in a similar fashion to the Perkin-Elmer Lambda 950™ mentioned above.

The second technique used the Lambda 950™ itself with an additional rotating center mount made by Labsphere to extend the capability of their basic integrating sphere accessory. This set-up has a few problems that make it more difficult to obtain a correct result than with the specialized instrument at Uppsala. There are several entrance ports which results in an uneven sphere wall. The detectors are baffled with respect to the normal use of the sphere so that the specular reflection enters the detector's field of view at oblique angles of incidence. The detectors are situated in the bottom of the sphere and looks straight at the center mount sample holder, hence it directly shades a large part of the detector's field of view. For the analysis of these measurements a power factor was introduced with respect to the correction of the sphere wall reflectance, this power factor was chosen so that the Spectralon absorption bands near 2000 nm disappeared from the slat reflectance spectra. A "third" technique is to use the Lambda 950™ in it's native mode without center mount as an additional check at normal incidence only.

There is some discrepancy in absolute reflectance between the two instruments, as shown in Figure 7, but the trend is clear: there is no significant change in direct-hemispherical reflectance with increasing angle of incidence for the high reflecting materials. The colored slats show an increase in reflectance above 60 degrees angle of incidence. However, the cross section of the slat decreases with increasing angle of incidence, so for the reference cases in the ISO 15099 only a small part of the direct light actually hits the slats these angles, most of the incident light is transmitted through. Second and higher order reflections also have low probability of interacting with a slat,

hence further reducing the influence of a change in reflection. With this assurance we can proceed for now with the usual assumption of constant reflectance in our models and simulations.

COMPARISON OF RADIOSITY AND RAYTRACING RESULTS

First, we compare results from the Window 6.0 implementation of the ISO 15099 framework to the table of sample results given in the ISO 15099 standard itself which was apparently produced using the WIS computer program (Rosenfeld, et al., 2000). Directional hemispherical values are compared in Table 1. Further breakdown of these results by optical component can be found in Carli (2005), but the bottom line is clear from this one table, i.e., values from ISO 15099 are reproduced usually to the third decimal place. The greatest deviations are found for configuration D45, which has partially transparent slats both in the solar and infrared. Such a product is unlikely to exist; any plastic thick enough to be rigid will be opaque in the thermal infrared. We shall therefore put case D45 aside for the remainder of this paper. While encouraging, this agreement so far only demonstrates that we have been able to correctly follow the general guidelines of ISO 15099 (and to avoid programming errors).

Now let us compare hemispherically integrated raytracing results with the basic Window 6.0 radiosity model. Figure 8 and Figure 9 show that Window 6.0 and TracePro® produce nearly identical results for directional hemispherical transmittance and reflectance, respectively, for the full range of possible incoming directions. The cyclic nature of the graph results from the fact that we are first sweeping through a full-circle of azimuth angles before moving on to the next highest altitude level. Each of these constant-θ “rings” produces a similarly shaped feature in the plot with increasing

amplitude at higher values of θ. Blinds with a 45° slat angle look much more transparent from below (peaks) than from above (valleys). The agreement is also excellent for each of the other example configurations listed in ISO 15099. Varying reflectance of the slats has little effect on blind transmittance (Figure 10) for most incoming angles at a given slat angle (A45, B45, C45). The single ISO configuration with a higher slat angle (C80), for which the blind is almost closed, has very low transmission except for the special case where light comes directly through the small gap from below.

Having demonstrated agreement for directional-hemispherical properties, let us begin to test the extensions of Window 6.0 to bidirectional properties. A first step should be to make sure that the distribution of the light into outgoing directions will add up to the hemispherical output of the ISO 15099 isotropic radiosity model. In the case of what we call the Uniform-Diffuse distribution in Window 6.0 this is a trivial exercise since the light is evenly distributed over the hemisphere. For the Directional-Diffuse model we are pleased to note that reintegrating the bidirectional values also closely reproduces the hemispherical values. With the integration checksum out of the way we can now examine the bidirectional distributions produced by Window 6.0. The Uniform Diffuse distribution will of course be far from correct in the case of a Venetian blind with its highly directional properties and we will not bother to compare it to raytracing. The more sophisticated Directional-Diffuse distribution has a chance to produce reasonable results.

In the figures that follow we display the results as a false-color hemisphere divided into patches for particular directions. The color of the patch represents the magnitude of the transmitted or reflected radiation. Each hemisphere represents the

outgoing transmitted or reflected radiance as specified for a given incident direction. The pole of the hemisphere represents light emerging in a normal direction to the vertical plane of the blind (θ=90°). The azimuthal angle φ=90° is pointing up. A full graphical description of a single blind configuration would require many such hemispheres; one for each incident direction.

Normal-incidence transmittance for ISO blind configuration A45 is displayed in Figure 11 using the directional diffuse enhancement to the ISO model. There is a typical bright first-reflection redirected region against a relatively uniform background. The directional diffuse model is so close to raytracing that it would be difficult to distinguish the differences by direct comparison between Figure 11 and a similar graph produced by raytracing on the same scale. Instead, in Figure 12 we display the differences between the two models plotted on an expanded scale. The greatest differences appear in the region near the boundary of the bright patches and diffuse background. This shows that the contrast between the bright and diffuse areas is somewhat more stark in the simplified Window 6.0 model. Intensity levels predicted by Window 6.0 however are now probably close enough for accurate calculation of solar heat gain in a multilayer glazing/shading system and possibly close enough for daylight distribution in many cases. A similar comparison is made in Figure 13 and Figure 14 for the case of reflectance. Again there are a few areas of relatively poor agreement near the transition from light to dark, but they have been reduced to low absolute levels.

Finally, we vary some of the blind parameters beyond the limitations of Window 6.0. Following ISO 15099, Window 6.0 breaks the slat into 5 segments, for each of which a view factor is formulated. Unlike the original framework, however, Window 6.0 allows

the slat segments to be oriented such that the slat can have a "curvature". Slat thickness is not currently an option in Window 6.0, although this extension is possible for a radiosity model. We can introduce slat thickness into the raytracing model to test the effect. As one might expect we find in general that introducing a thickness that is much smaller than the slat width has a negligible change in the results of raytracing. There are some cases, however, where the slat cross section just happens to block some of the directly transmitted light which can cause a large perturbation from the zero-thickness case. For example, if the A45 case is raytraced with 0.01 mm-thick slats and then increased to 1.0 mm, the directly transmitted component is reduced from 0.057 to zero. This is a large relative change since the diffusely reflected component of blind transmission is only 0.198.

Specularity of the slats must affect the results in terms of directionality, even if not in total throughput. Furthermore, there may well be combined effects of specularity and curvature. Unlike thickness or curvature alone, the specularity effect could not be added to the radiosity model directly, although perhaps a simplified raytracing model could be be added in parallel. From the base case of a perfectly diffuse slat material with a reflectance of 0.7 similar to white paint (case A45) we increase the specularity from zero to 20% and then to 80%. In magnitude the directional hemispherical values are little changed at the 20% specularity level (Figure 15). At the 80% specularity level however there are significant differences especially at the lower and higher values of θ. At low θ (near-normal incidence) the transmittance is always higher for the highly specular case as more light is guided through the slats without dispersion. At higher values of θ, and at φ values such that the light comes from below, the specular blinds can have lower

transmittance when light is reflected back outside on the first bounce. More striking differences are seen in the distribution of transmitted light in Figure 16 and Figure 17. Again the 20% specular case is only slightly distorted from the perfectly diffuse case, but now the 80% specular blind is not even qualitatively similar.

CONCLUSIONS

The radiosity model of Window 6.0 based on ISO 15099 is found to be a highly accurate method for predicting the hemispherical transmission and reflection of slat shading systems. Using an extension to the base model, Window 6.0 also accurately predicts the distribution of radiation with only minor deviations near the directions with high gradients. One exception is the use of slat materials with a strong specular component of reflectance. In these cases even the hemispherical transmittance and reflectance can be significantly in error and the directional behavior will be poorly represented. For specular blinds we must rely on raytracing to generate full bidirectional properties which can then be stored in the Window 6 layer database.

ACKNOWLEDGEMENTS

This work was supported by the Assistant Secretary for Energy Efficiency and Renewable Energy, Office of Building Technology, Building Technology Programs of the U.S. Department of Energy under Contract No. DE-AC03-76SF00098. TracePro® is a registered trademark of Lambda Research Corporation. Some of the optical data was obtained using the facilities of the Ångström Laboratory at Uppsala University in Sweden with the kind cooperation of Prof. Arne Roos.

REFERENCES

Andersen, M., Rubin, M., and Scartezzini, J.L., 2005a. Comparison between ray-tracing simulations and bi-directional transmission measurements on prismatic glazing, Solar Energy **74,** 157-173.

Andersen, M., Rubin, M., Powles, R., Scartezzini, J.-L., 2005b Bi-directional transmission properties of Venetian blinds: experimental assessment compared to ray-tracing calculations, Solar Energy **78,** 187-198

Campbell, N.S. and Whittle, J.K. 1997. Analysing Radiation Transport through Complex Fenestratioin Systems, Proc. IBPSA Building Simulation '97, Czech Technical Univ., Prague.

Carli, Inc., 2005. Tarcog and Venetian characterization results, Technical Report, Carli. Inc., Amherst MA.

Carli, Inc., 2006. Technical Report: Calculation of Optical Properties for a Venetian Blind Type of Shading Device, Carli Inc., Amherst MA.

ISO 15099 (2002). Thermal Performance of Windows, Doors and Shading Devices – Detailed Calculations. ISO Standard.

Mitchell, R., Kohler, C., Klems, J., Rubin, M., and Arasteh, A., Huizenga, C., Yu, T., Curcija, D. , 2006. WINDOW 6 / THERM 6 Research Version User Manual, LBNL Report 941, Lawrence Berkeley National Laboratory, University of California, Berkeley CA USA. http://windows.lbl.gov/software/software.html

Klems, J.H., 1994. A New Method for Predicting the Solar Heat Gain of Complex Fenestration Systems. ASHRAE Trans., 100, Pt 1 and Pt. 2.

Klems, J.H., 2004a. Angular bases for bidirectional calculation, LBNL Report (unpublished).

Klems, J.H., 2004b. Detailed Equations for Connecting a 2D Blind Model with the Bidirectional Calculation, LBNL Report.

Klems, J. H., 2005. Calculating Outgoing Radiance in the 2D Venetian Blind Model, LBNL Report.

Kuhn, T.E., Buhler, C., and Platzer, W.J., 2000. Evaluation of Overheating Protection with Sun-Shading Systems, Solar Energy 69 (Suppl.) 59-74.

Mitts, S.J. and Smith, T. April 1985. Radiative Propertis of Space Systems with Extension to Variable Slat Properties, Technical Report ME-TFS-003-85, Dept. of Mech. Eng., Univ. of Iowa, Iowa City.

Nostell, P., Roos, A., Rönnow, D., 1999. Single-beam integrating sphere spectrophotometer for reflectance and transmittance measurements versus angle of incidence in the solar wavelength range on diffuse and specular samples, Rev. Sci. Instr., 70, (5), 2481-2494.

Parmelee, G.V and Aubele, W. W., 1952. The Shading of Sunlit Glass – An Analysis of the Effect of Uniformly Spaced Flat Opaque Slats, A.S.H.V.E. Trans. 58, 327.

Platzer, W.J., 19-22 June 2000. The ALTSET Project: Measurement of Angular properties for Complex Glazing. Proc. 3rd Int. ISES Europe (Eurosun) Conf., Copenhagen, Denmark.

Rosenfeld, J.L.J., Platzer, W.J., Van Dijk, H., and Maccari, A., 2000. Modeling the Optical and Thermal Properties of Complex Glazing: Overview of Recent Developments, Solar Energy 69 (Suppl.) 1-13.

Siegel, R. and Howell, J.R. , 1981. Thermal Radiation Heat Transfer, second ed. McGraw-Hill, New York.

Tregenza, P.R., 1987. Subdivision of the sky hemisphere for luminance measurements, Lighting Research and Technol., vol. 19 (H.1), pp 13-14.

Van Dijk, D., and Bakker, L., 1998. The Characterization of the Daylighting Properties of Special Glazings and Solar Shading Devices, Proc. of EuroSun98, Portoroz, Slovenia.

TABLES

Table 1. ISO blind configurations and comparison of the directional hemispherical transmittance and reflectance produced by Window 6.0 and appearing in ISO 15099. In the configuration column, "top" refers to the convex surface of the slat that normally faces outward and "front" refers to the outward face of the blind.

Blind configuration ID		A45		B45		C45		C80		D45	
Slat top surface		white		pastel		white		white		translucent	
Slat bottom surface		white		pastel		dark		dark		translucent	
Slat spacing (mm)		12		12		12		12		12	
Slat width (mm)		16		16		16		16		16	
Slat tilt angle (deg.)		45		45		45		80		45	
solar trans.		0.00		0.00		0.00		0.00		0.40	
Solar refl. (front)		0.70		0.55		0.70		0.70		0.50	
Solar refl. (back)		0.70		0.55		0.40		0.40		0.50	
IR trans.		0.00		0.00		0.00		0.00		0.40	
IR emit. (front)		0.90		0.90		0.90		0.90		0.55	
IR emit. (back)		0.90		0.90		0.90		0.90		0.55	
Solar incidence angle		0	60	0	60	0	60	0	60	0	60
Solar "dir-dif" trans. (front)	ISO	0.141	0.073	0.090	0.047	0.096	0.051	0.012	0.005	0.373	0.277
	W6	0.1407	0.0730	0.0903	0.0472	0.0957	0.0508	0.0109	0.0048	0.3733	0.2756
Solar "dir-dif" trans. (back)	ISO	0.141	0.288	0.090	0.216	0.076	0.271	0.011	0.027	0.373	0.306
	W6	0.1407	0.2882	0.0903	0.2161	0.0759	0.2714	0.0101	0.0268	0.3733	0.3063
Solar "dir-dif" refl. (front)	ISO	0.394	0.558	0.295	0.430	0.371	0.544	0.622	0.678	0.418	0.567
	W6	0.3936	0.5587	0.2952	0.4308	0.3707	0.5454	0.6308	0.6788	0.4184	0.5676
Solar "dir-dif" refl. (back)	ISO	0.394	0.103	0.295	0.066	0.216	0.070	0.356	0.273	0.418	0.273
	W6	0.3936	0.1030	0.2952	0.0661	0.2158	0.0701	0.3605	0.2735	0.4184	0.2733

FIGURE CAPTIONS

FIGURES

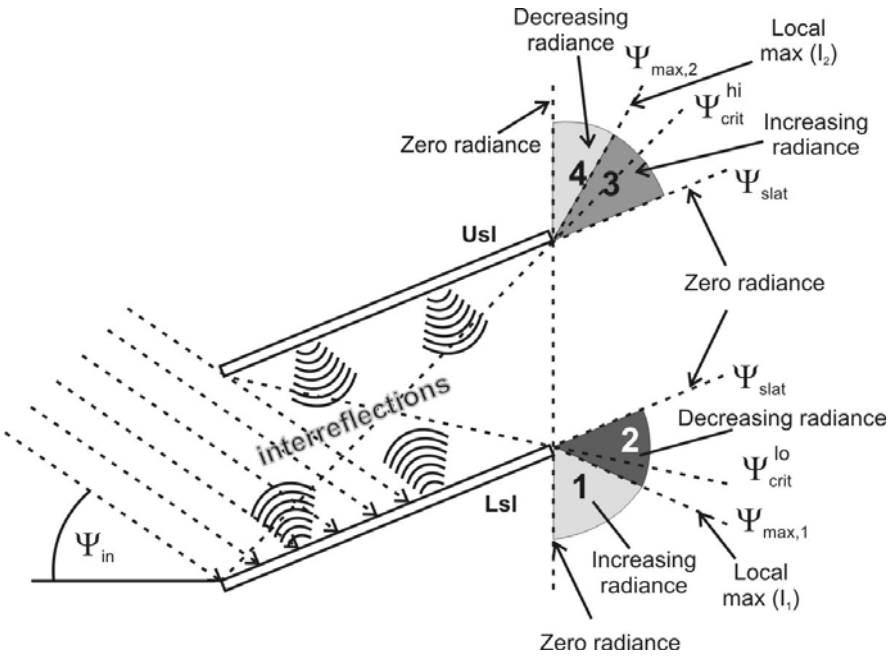

Figure 1. Distribution of transmitted radiance into zones by consideration of cutoff angle.

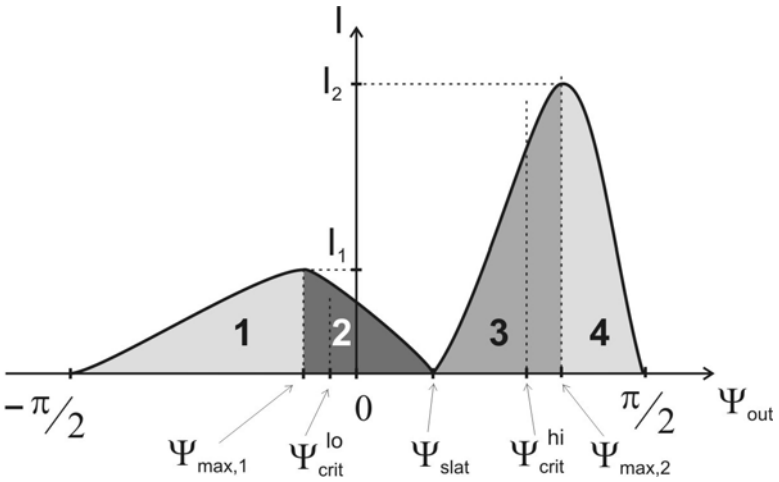

Figure 2. Outgoing radiance versus outgoing profile angle for directional-diffuse transmittance.

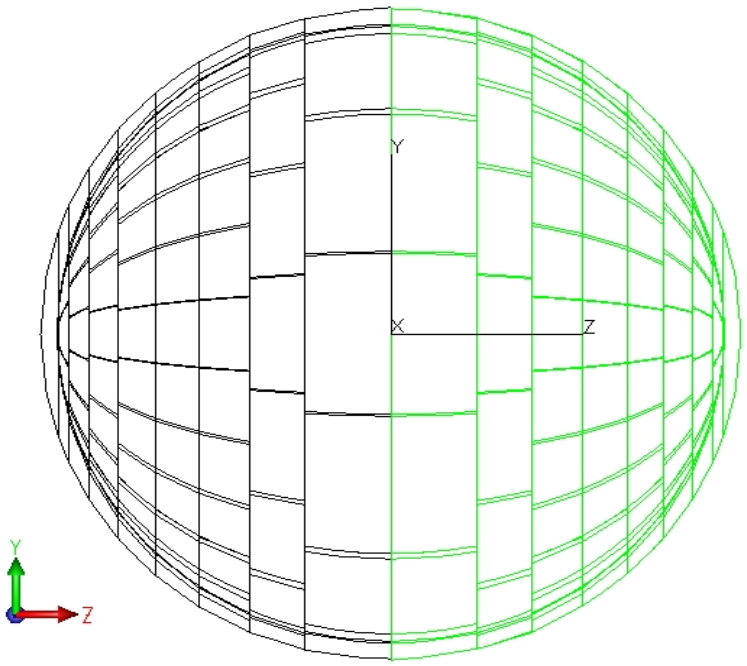

Figure 3. A segmented detector array created by subtracting planes from a spherical shell.

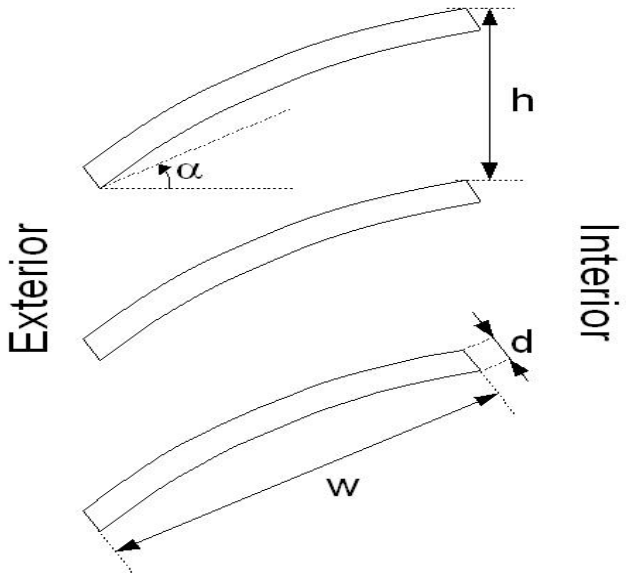

Figure 4. A Venetian blind diagram generated by a script.

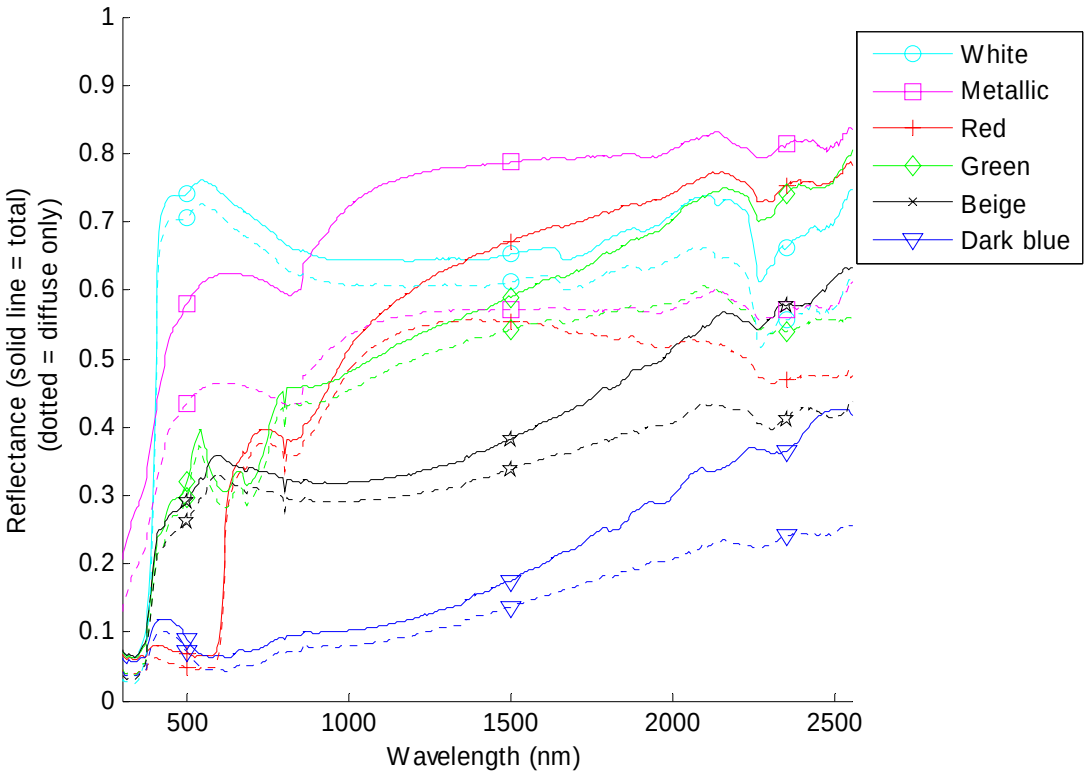

Figure 5. Near-normal to hemispherical reflectance of slat surfaces painted in various colors.

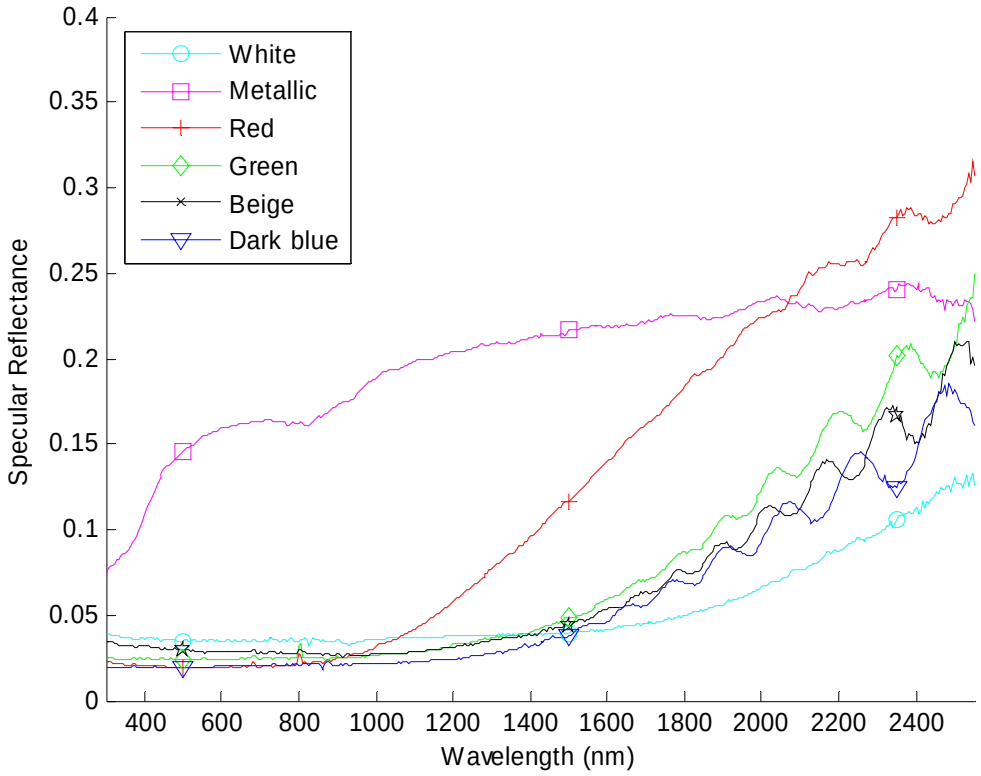

Figure 6. Near-normal specular reflectance of slat surfaces painted in various colors.

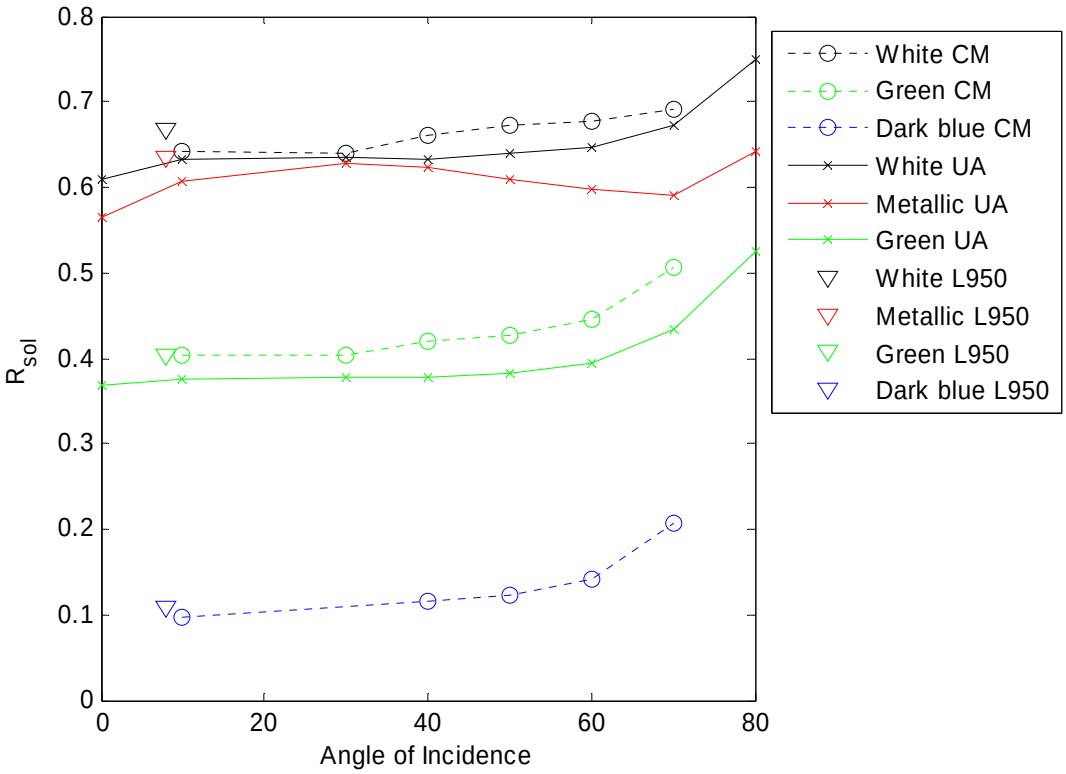

Figure 7. The average solar reflectance of four slat materials versus angle of incidence . Two instruments were used: a commercial spectrometer with a center mount integrating sphere (CM) and a specialized instrument at Uppsala (UA). Triangles show reflectance values obtained with the spectrometer in normal operating mode without center mount.

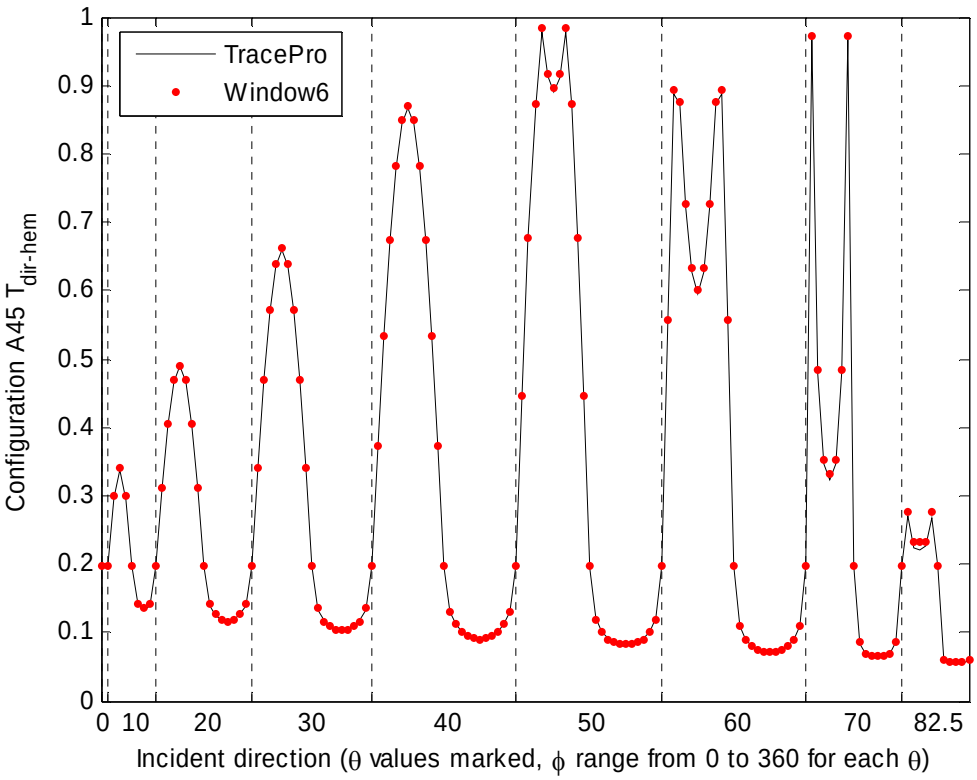

Figure 8. Comparison of directional-hemispherical transmittance calculated by Window 6.0 and TracePro® for ISO blind configuration A45. The vertical lines bound cycles of φ from 0 to 360 degrees for the labeled band of θ. The two curves are so closely overlaid that the difference can only be seen at the highest theta.

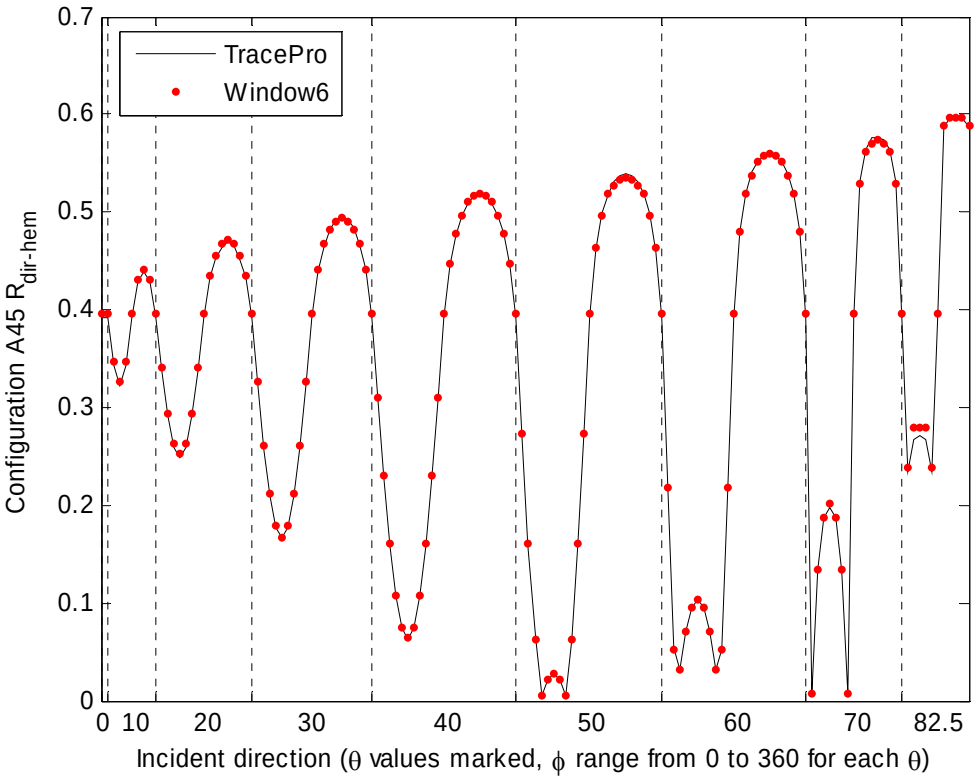

Figure 9. Comparison of directional-hemispherical reflectance calculated by Window 6.0 and TracePro® for ISO blind configuration A45. The vertical lines bound cycles of φ from 0 to 360 degrees for the labeled band of θ.

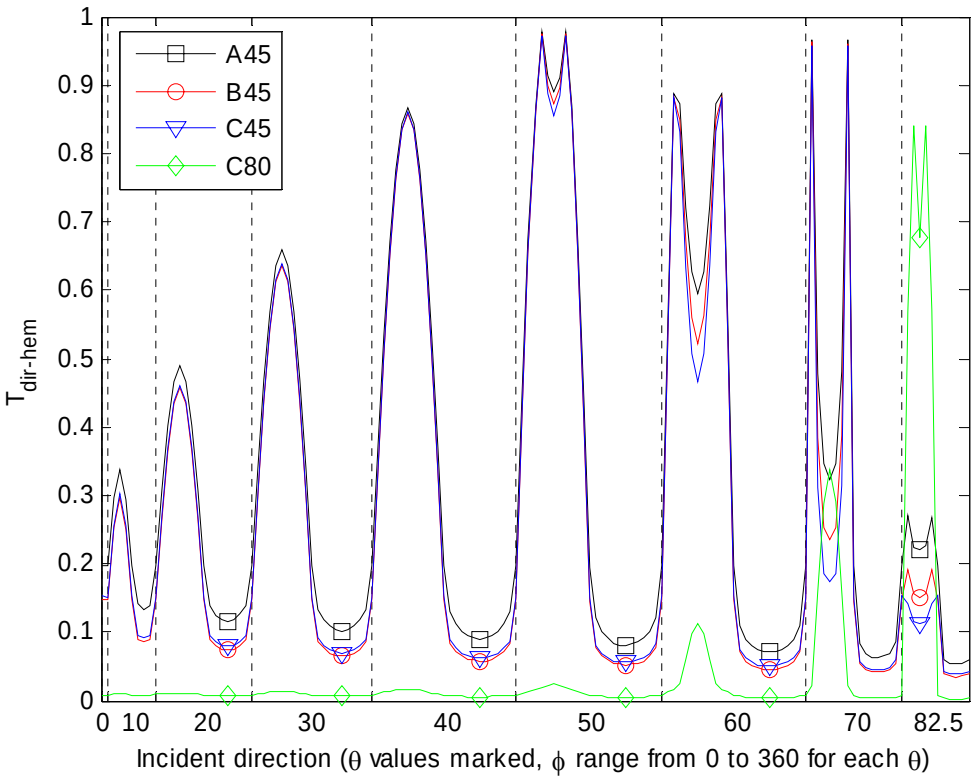

Figure 10. Directional-hemispherical transmittances for each of the ISO blind configurations.

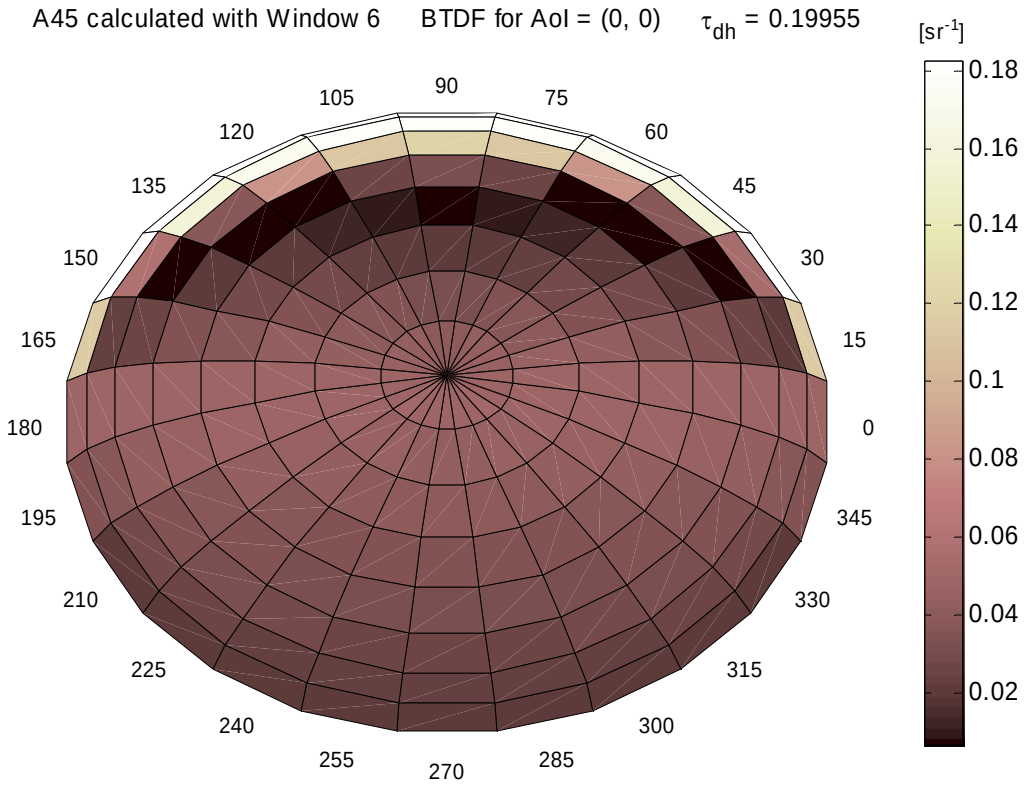

Figure 11. Transmittance distribution for ISO blind configuration A45 calculated using Window 6.0 at normal incidence.

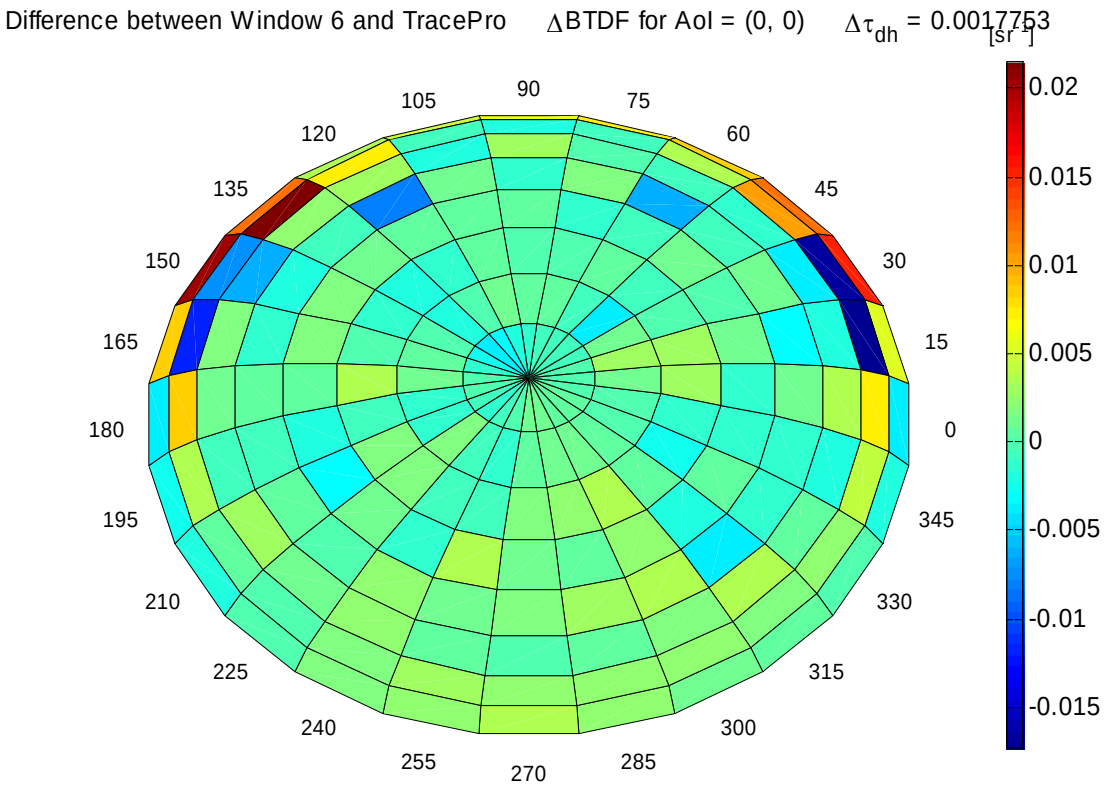

Figure 12. Differences between Window 6.0 radiosity model and TracePro Monte Carlo model for transmission at normal incidence.

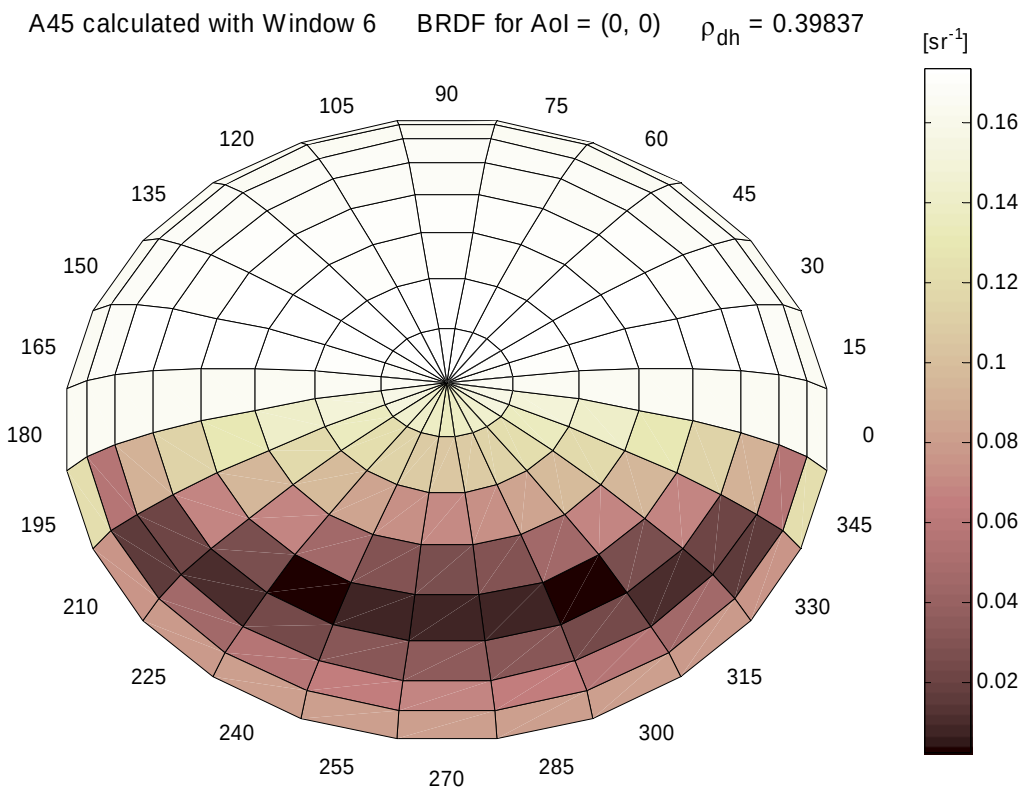

Figure 13. Reflectance distribution for ISO blind configuration A45 calculated using Window 6.0 at normal incidence.

.

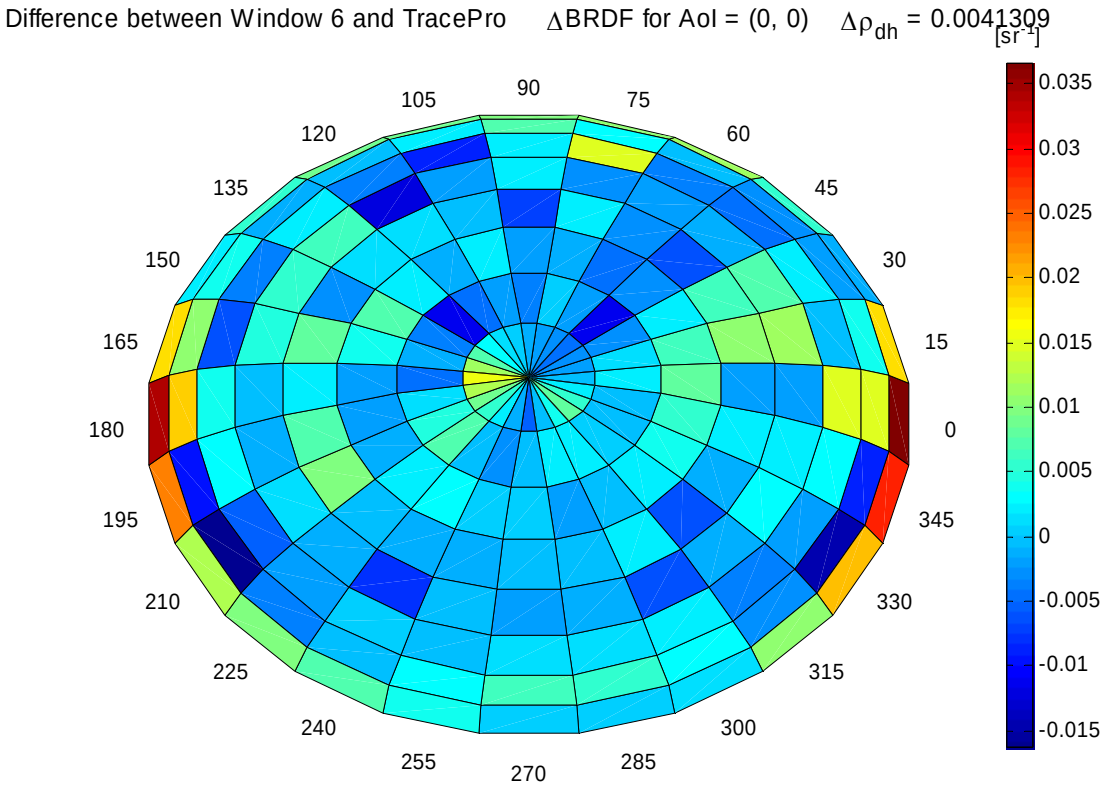

Figure 14. Difference between the Windos 6.0 radiosity model and the TracePro Monte Carlo model for ISO configuration A45 for reflection at normal incidence.

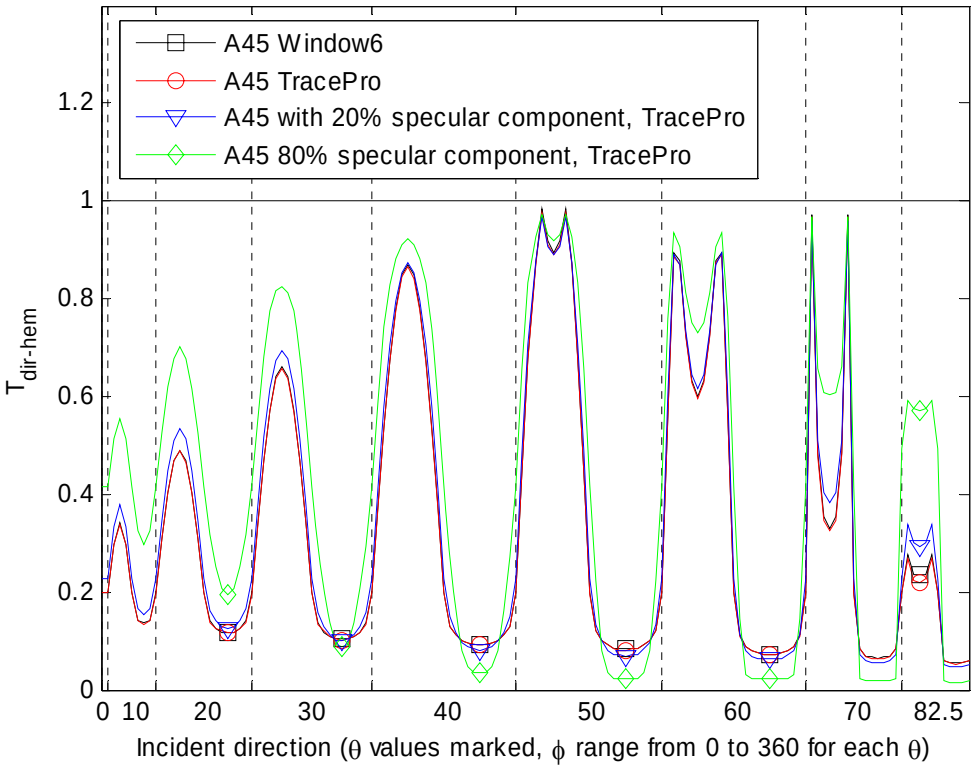

Figure 15. Directional-hemispherical transmittance for blind A45 and modifications to 20% and 80% specular slat reflectivity.

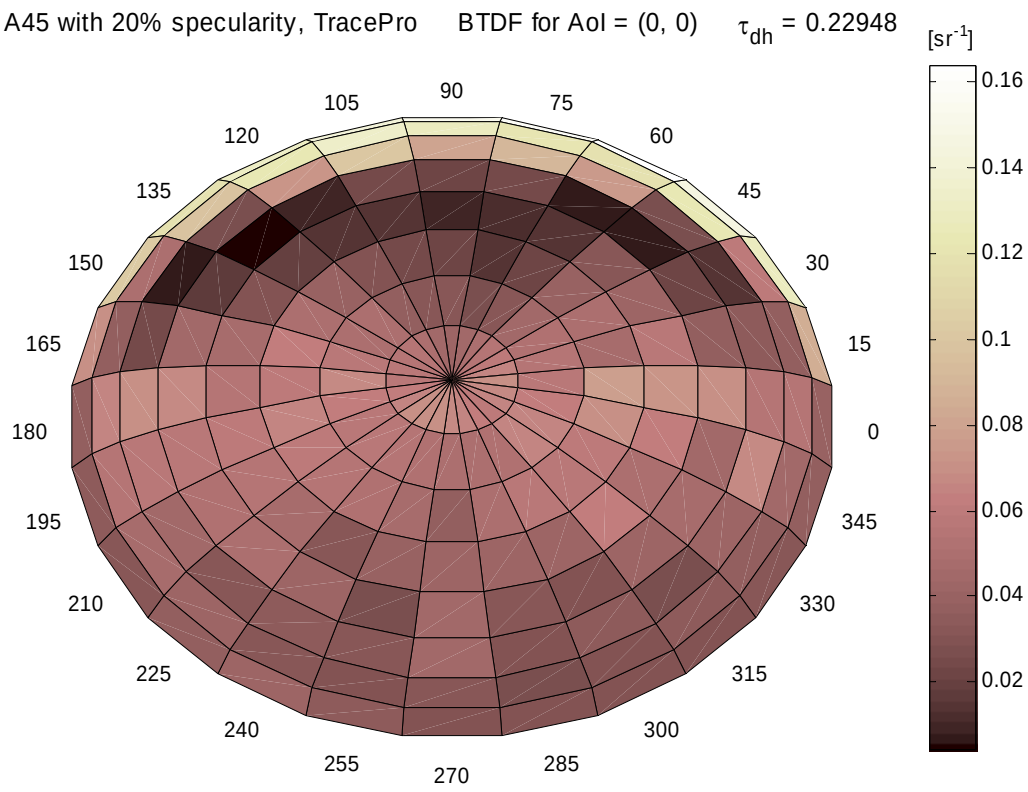

Figure 16. Bidirectional transmittance for blind A45 with 20% specular slats

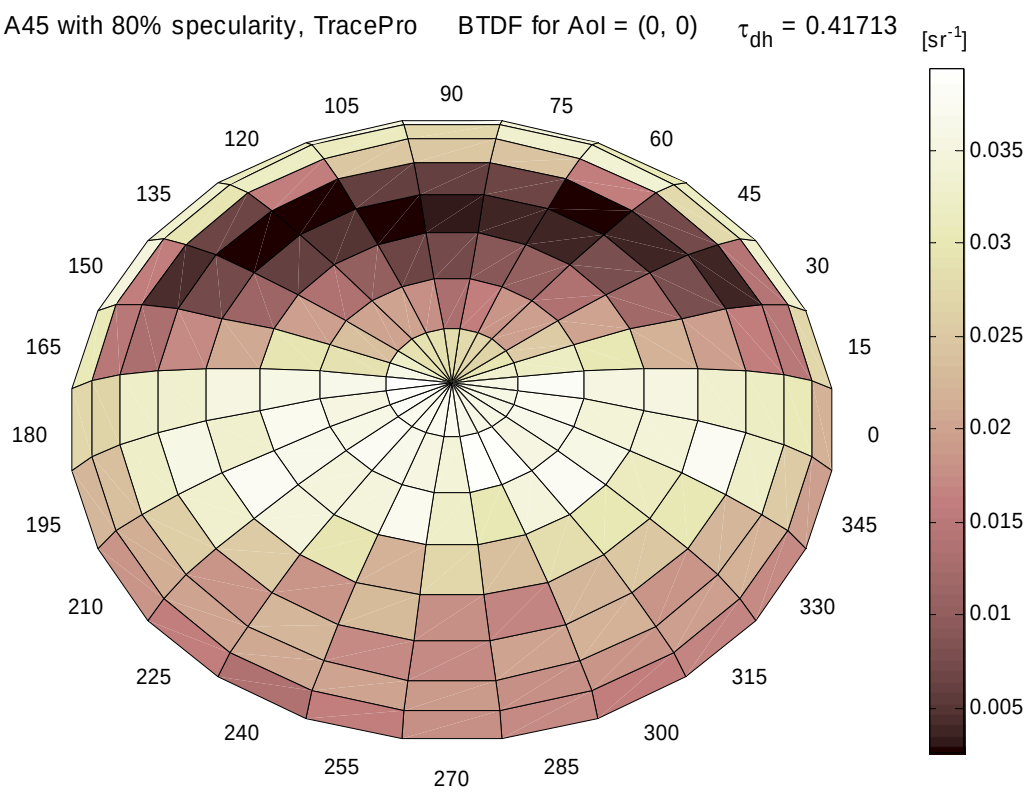

Figure 17. Bidirectional transmittance for blind A45 with 80% specular slats